2012

Snow Cover Monitoring from Remote-Sensing Satellites: Possibilities for Drought Assessment

Cezar Kongoli
National Oceanic and Atmospheric Administration

Peter Romanov
National Oceanic and Atmospheric Administration

Ralph Ferraro
National Oceanic and Atmospheric Administration

Published in *Remote Sensing of Drought: Innovative Monitoring Approaches,* edited by Brian D. Wardlow, Martha C. Anderson, & James P. Verdin (CRC Press/Taylor & Francis, 2012).

Authors:

Cezar Kongoli
National Environmental Satellite, Data, and Information Service
National Oceanic and Atmospheric Administration
Camp Springs, Maryland

Peter Romanov
National Environmental Satellite, Data, and Information Service
National Oceanic and Atmospheric Administration
Camp Springs, Maryland

Ralph Ferraro
National Environmental Satellite, Data, and Information Service
National Oceanic and Atmospheric Administration
Camp Springs, Maryland

15 Snow Cover Monitoring from Remote-Sensing Satellites

Possibilities for Drought Assessment

Cezar Kongoli, Peter Romanov, and Ralph Ferraro

CONTENTS

15.1 INTRODUCTION

Snow cover is an important earth surface characteristic because it influences partitioning of the surface radiation, energy, and hydrologic budgets. Snow is also an important source of moisture for agricultural crops and water supply in many higher latitude or mountainous areas. For instance, snowmelt provides approximately 50%–80% of the annual runoff in the western United States (Pagano and Garen, 2006) and Canadian Prairies (Gray et al., 1989; Fang and Pomeroy, 2007), which

substantially impacts warm season hydrology. Limited soil moisture reserves from the winter period can result in agricultural drought (i.e., severe early growing season vegetation stress if rainfall deficits occur during that period), which can be prolonged or intensified well into the growing season if relatively dry conditions persist. Snow cover deficits can also result in hydrological drought (i.e., severe deficits in surface and subsurface water reserves including soil moisture, streamflow, reservoir and lake levels, and groundwater) since snowmelt runoff is the primary source of moisture to recharge these reserves for a wide range of agricultural, commercial, ecological, and municipal purposes. Semiarid regions that rely on snowmelt are especially vulnerable to winter moisture shortfalls since these areas are more likely to experience frequent droughts. In the Canadian Prairies, more than half the years of three decades (1910–1920, 1930–1939, and 1980–1989) were in drought. Wheaton et al. (2005) reported exceptionally low precipitation and low snow cover in the winter of 2000–2001, with the greatest anomalies of precipitation in Alberta and western Saskatchewan along with near-normal temperature in most of southern Canada. The reduced snowfall led to lower snow accumulation. A loss in agricultural production over Canada by an estimated $3.6 billion in 2001–2002 was attributed to this drought. Fang and Pomeroy (2008) analyzed the impacts of the most recent and severe drought of 1999/2004–2005 for part of the Canadian Prairies on the water supply of a wetland basin by using a physically based cold region hydrologic modeling system. Simulation results showed that much lower winter precipitation, less snow accumulation, and shorter snow cover duration were associated with much lower discharge from snowmelt runoff to the wetland area during much of the drought period of 1999/2004–2005 than during the nondrought period of 2005/2006.

Given the importance of snowmelt and its potential impact on water resources of snow-covered regions, the monitoring of snow is an integral part of water management in these regions. Hydrologically important snowpack measurements are the snow water equivalent (SWE), snow depth (SD), and snow-covered area (SCA). SWE refers to the amount of water (frozen and liquid) contained in the snowpack (calculated from SD multiplied by effective snow cover density). It is the most important snow parameter for snowmelt runoff forecasting before the onset of snowmelt season. For example, in the western United States and Alaska, the U.S. Department of Agriculture (USDA) Natural Resources Conservation Service (NRCS) maintains an automated SWE monitoring system called SNOwpack TELemetry (SNOTEL) and a network of manual snow courses that complement SNOTEL, which are used in combination with other climatological and streamflow data to create water supply forecasts (Pagano and Garren, 2006). SD is physically related to SWE and is routinely measured from ground-based meteorological stations. Daily observations of SD have been made dating from the late 1800s in a few of these countries (e.g., Switzerland, United States, former Soviet Union, and Finland). SCA indicates the spatial extent or fraction of land surface covered by snow. SCA monitoring can be used to estimate the snow duration, which has a stronger physical relationship with both SD and SWE. For example, in areas where the average winter temperature is below or close to the freezing point, moisture in the snowpack gradually accumulates throughout the winter season, and longer snow duration typically results in larger SWE by the beginning of spring snowmelt. Abnormally short duration of

snow cover may be indicative of the lack of winter precipitation and therefore may be considered an early indicator of potential early spring drought.

The spatial distribution of ground-based stations measuring SD and SWE is generally skewed to low elevation regions of the Northern Hemisphere midlatitudes and to snow courses in mountainous regions. Also, most stations are located in relatively close proximity to urban areas for access purposes, and thus large geographic expanses may go unmonitored. In addition, the current tendency to reduce the number of manual stations and to replace manual stations with automated ones results in a continuous reduction in the amount of available ground-based information on snow, because some automated stations are not equipped with SD sensors. Satellite observations, on the other hand, can complement surface observations by providing information on the snow cover distribution and seasonal change with much-improved spatial coverage and temporal frequency that cannot be matched by in situ measurements.

In this chapter, the main satellite remote-sensing methods and applications for snow cover monitoring are reviewed, with an emphasis on the monitoring of SCA, SWE, and SD parameters. First, an overview of snow cover monitoring using optical imagery is provided, including a discussion of the main physical principles and sensor characteristics, operational products, and validation studies. Snow cover monitoring using passive microwave (MW) imagery is then summarized in a similar fashion, with additional discussion of data assimilation techniques used for improved monitoring of SWE and SD, which cannot be accomplished solely by optical or MW remote-sensing methods with sufficient accuracy. Multisensor blending techniques that utilize information from visible, infrared (IR), and MW observations are then described. Lastly, an example of applying remote sensing for SCA monitoring and early drought prediction is presented over the Ukraine.

15.2 SNOW MAPPING WITH OPTICAL SATELLITE OBSERVATIONS

15.2.1 Physical Principles and Sensor Characteristics

Snow is among the most "colorful" natural materials (Dozier et al., 2009) in that it possesses a strong spectral gradient in reflectance ranging from a high reflectance (albedo) in the visible wavelengths to low reflectance in the middle IR wavelengths (Wiscombe and Warren, 1980). Figure 15.1 shows plots of modeled spectral distribution of snow reflectance in the visible (0.4–0.7 μm) and near (0.7–1.3 μm) and middle (1.3–2 μm) IR wavelengths for a range of snow grain sizes. As shown, snow reflectance is high and relatively insensitive to grain size in the visible range, whereas reflectance decreases and its sensitivity to grain size increases dramatically in the near and middle IR ranges. This characteristic spectral response in the optical wavelengths distinguishes snow from most other natural surfaces (e.g., soil, water, and vegetation), as shown in Figure 15.2. In the far IR wavelengths (not shown), snow emits thermal radiation close to that of a blackbody, and, thus, its brightness temperature as observed by the satellite sensor depends mainly on the physical temperature of the top thin layer of the snowpack. In these wavelengths, the snow brightness temperature is relatively low, which is also useful information for snow identification.

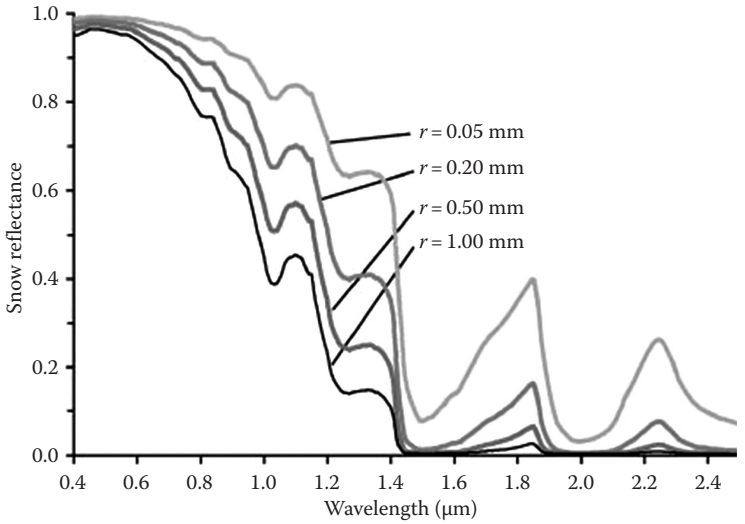

FIGURE 15.1 Snow reflectance spanning the visible, near-IR, and mid-IR wavelengths for a range of snow grain sizes (*r*). (From Dozier, J. and T.H. Painter, *Annu. Rev. Earth Planet. Sci.,* 32, 465, 2004.)

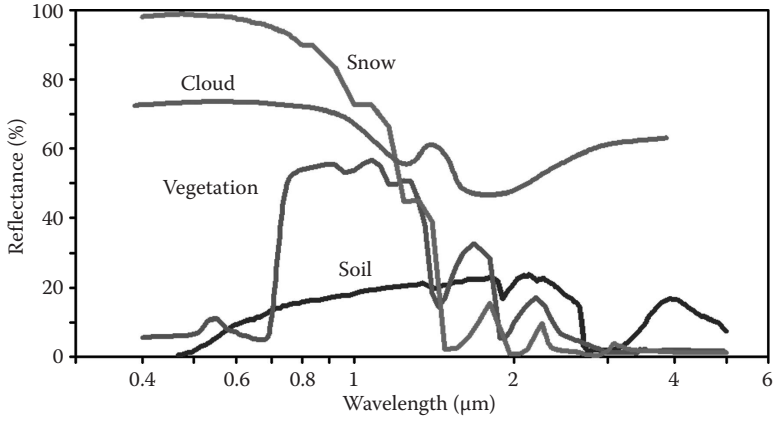

FIGURE 15.2 **(See color insert.)** Spectral reflectance for different land surface cover types including snow.

Most current meteorological satellite instruments collect observations in spectral regions centered in the visible at around 0.6 μm, the middle IR at 1.6 μm and 3.7–3.9 μm, and the thermal IR at 10–12 μm. Therefore, data collected from these instruments can generally be used to identify snow and map snow cover distribution. Snow retrievals from satellite optical measurements require clear sky conditions and sufficient daylight.

The purpose of satellite-based snow identification and mapping algorithms is to distinguish snow-covered land surface from snow-free land and clouds. Automated

algorithms to identify snow usually incorporate a set of threshold tests that utilize satellite-observed reflectance and brightness temperature values in the spectral bands mentioned earlier, along with specific spectral indices. The Snow Index (SI), defined as a simple ratio of the reflectance in the visible (R_{vis}) and middle IR (R_{mir}), has been applied to identify snow in the algorithm described in Romanov et al. (2000). The snow detection algorithm of Hall et al. (2002) uses the normalized difference between reflectance in the visible and middle IR called the Normalized Difference Snow Index (NDSI):

$$\mathrm{NDSI} = \frac{R_{vis} - R_{mir}}{R_{vis} + R_{mir}} \tag{15.1}$$

Clouds and snow-free land surfaces typically exhibit lower values of SI and NDSI than snow-covered land. In the snow-mapping algorithm of Hall et al. (2002), cloud-free pixels having an NDSI value >0.4, a visible reflectance >11%, and IR brightness temperature below 283 K are classified as snow covered.

The accuracy of snow cover maps can be affected by clouds that exhibit spectral features similar to snow, because such clouds may be misidentified as snow by the automated algorithm. Masking of snow cover by forest canopy changes the spectral reflectance of the scene by decreasing reflectance in the visible band and increasing it in the middle IR. Very dense boreal forests may mask the snow cover on the forest floor almost completely and therefore prevent proper snow detection and mapping with satellite data. The SD and SWE parameters are not typically retrieved from optical imagery since the snow reflectance is influenced by only a shallow layer of snow.

15.2.2 Primary Optical-Based Products

Optical measurements from earth-observing satellites present an important tool for monitoring SCA. The large number of satellite sensors providing measurements in the visible and IR spectral range, the relatively high spatial resolution of observations (1–4 km), and the relatively simple physical background of snow remote-sensing techniques are among the primary factors that explain widespread interest in using satellite optical data to develop snow products.

Identification of snow in satellite imagery by visual analysis and interpretation is the oldest snow-mapping technique. Since 1972, this approach has been routinely used by the National Oceanic and Atmospheric Administration (NOAA) to generate weekly maps of snow and ice distribution in the Northern Hemisphere. In 1999, the computer-based Interactive Multisensor Snow and Ice Mapping System (IMS) was implemented to facilitate image analysis by human analysts (Ramsay, 1998). This improved the nominal spatial resolution of the maps from 180 to 24 km and the temporal resolution from weekly to daily snow-mapping updates. In 2004, the spatial resolution of the IMS snow products was further increased to 4 km (Helfrich et al., 2007).

When mapping snow cover with IMS, analysts rely primarily on the visible imagery from polar-orbiting and geostationary satellites. The imagery from geostationary satellites is utilized in the form of animations, which help to distinguish moving clouds

from snow. Quite often, analysts visually observe and map the distribution of snow cover through semitransparent clouds. This is an obvious advantage compared to automated techniques based on optical measurements (discussed later in this section) where practically any cloud prevents a reliable characterization of the state of the land surface. Since 2006, the upgraded IMS has had access to several automated snow and ice products generated at NOAA and the National Aeronautics and Space Administration (NASA), as well as surface in situ SD reports. Recently analysts also started using images from live-streaming web cameras throughout the world. Availability of these additional sources of information has substantially enhanced the potential of analysts to accurately reproduce the snow cover distribution, especially in the case of persistent cloud cover when application of satellite visible imagery is ineffective.

Owing to a simple and straightforward satellite image analysis technique and to the use of several additional sources of information on snow, interactive snow cover maps present a consistent, robust, and highly accurate product. IMS maps of snow and ice cover are considered the primary NOAA snow cover product and are incorporated in all global and mesoscale operational numerical weather prediction models run by NOAA's National Centers for Environmental Prediction (NCEP). High-spatial-resolution 4 km IMS maps are updated daily, making them potentially useful for various environmental and practical applications at regional and local scales, including drought monitoring. With more than 35 years of continuous snow cover monitoring, NOAA snow charts also present a unique source of information for global climate change studies (Frei and Robinson, 1999). It is important to note, however, that the changes in both frequency of map generation and spatial resolution have introduced inhomogeneity in the time series and thus substantially reduced the climatological value of the IMS-derived data set (Frei, 2009). Since 2007, NOAA interactive snow cover maps are produced at the National Ice Center (NIC). Daily IMS products are archived and are available from the National Snow and Ice Data Center (NSIDC).

In contrast to interactive snow-mapping techniques (similar to IMS), automated algorithms can better utilize the advantages of satellite observations, including high spatial resolution, multispectral sampling, and a frequent-repeat observation cycle. In the last two decades, data from polar-orbiting satellites have been most frequently used for monitoring global snow cover. Since 2000, NASA has produced snow cover maps from observations of the Moderate Resolution Imaging Spectroradiometer (MODIS) onboard the Terra and Aqua satellites (Hall et al., 2002). A suite of MODIS snow products includes global maps of snow cover distribution generated at daily, 16 day, and monthly time steps at a spatial resolution ranging from 500 m to 20 km (http://modis-250 m.nascom.nasa.gov/cgi-bin/browse/browse.cgi). Several algorithms have been developed and applied to identify and map snow cover using the Advanced Very High Resolution Radiometer (AVHRR) sensor onboard NOAA polar-orbiting satellites (e.g., Simpson et al., 1998; Baum and Trepte, 1999). In 2006, an automated algorithm to identify snow cover in NOAA AVHRR imagery was implemented at NOAA/NESDIS and used to produce daily global snow cover maps at a 4 km spatial resolution (http://www.star.nesdis.noaa.gov/smcd/emb/snow/HTML/snow.htm).

Continuous observations from AVHRR onboard different NOAA satellites have been available since the late 1970s. This extended time series of AVHRR data represents a valuable source of information for snow climatology and climate change studies.

The Canadian Center for Remote Sensing (CCRS) has consistently reprocessed historical AVHRR data for the time period from 1982 to 2005 to establish snow cover climatology over Canada at 1 km resolution (Khlopenkov and Trishchenko, 2007), but no attempts to expand these efforts globally have been reported to date.

Most current imaging instruments onboard geostationary satellites provide observations in the visible, middle IR, and thermal IR spectral bands and thus also allow for automated snow cover identification and mapping. The area coverage of geostationary satellites is generally limited to the area between 65° North and 65° South latitude, and thus they can only be used for snow monitoring in the midlatitudes. A particular advantage of geostationary satellites is their frequent views, available typically at 15 or 30 min intervals. Frequent observations provide more cloud-free views during the day and thus help to improve the effective area coverage of the daily snow product. A practical way to utilize multiple views from geostationary satellites and to reduce cloud contamination in the snow map is to apply a maximum temperature image compositing technique (e.g., Romanov et al., 2000). For every pixel of an image, the observation with the highest IR brightness temperature acquired during the day is identified and retained. Since cloudy areas are typically associated with lower IR brightness temperatures, the maximum temperature tends to be associated with the most cloud-free observations available during the day. Since 1999, this technique has been routinely used by NOAA/NESDIS for generating automated 4 km snow cover maps over North America. Observations from the Spinning Enhanced Visible and IR Imager (SEVIRI) onboard another geostationary satellite, Meteosat Second Generation (MSG), have also been applied to routinely generate snow maps over Europe and Northern Africa (Romanov and Tarpley, 2006; de Wildt et al., 2007).

15.2.3 Validation of Optical Products

A traditional technique for estimating the accuracy of satellite-based snow maps consists of direct comparison with in situ, synchronous surface SD measurements. Daily SD reports from first-order stations across the globe and additional stations within regional networks (e.g., U.S. Cooperative Network stations) provide the means for year-round evaluation of the accuracy of snow cover products in different physiogeographic regions.

Hall and Riggs (2007) analyzed the validation results of the MODIS snow cover products from studies over several locations around the world and concluded that the accuracy of the 0.5 km resolution snow maps generally exceeds 94%. This estimate closely corresponds to the results of Simic et al. (2004), where MODIS maps were compared to SD reports from Canadian first-order and climate monitoring network stations. However, the latter work demonstrated that the accuracy of MODIS maps, as well as the accuracy of other satellite snow remote-sensing products, substantially decreased to 80%–85% over densely forested areas. Masking and shadowing of snow cover by the tree canopy along with littering of the snow by tree debris substantially reduce the visible reflectance of the snow-covered land surface and thus complicate proper identification of snow in heavily forested areas. The accuracy of snow identification also degrades over shallow or patchy snow cover since portions of the snow-free land along with vegetation protrusions through the snowpack make the scene look "darker" in the visible spectral bands. Ault et al. (2006) reported only

41% correspondence of MODIS snow maps to surface observations when only a trace amount of snow cover (<10 mm) was reported on the ground. Snow maps generated from geostationary satellite data provide a similar level of accuracy as the polar satellite data-based products. Romanov et al. (2000) compared GOES-based snow maps with observations from U.S. Cooperative Network stations over the continental United States and found the two data sets to have an average agreement of 88%.

The estimated accuracy of interactive snow cover maps is similar or slightly less than the accuracy of automated products based on optical data (e.g., Romanov et al., 2000). It is important, however, for the comparison of reported accuracy of automated and interactive snow maps to be performed with care. The accuracy of automated optical products characterizes snow retrievals only over limited cloud-clear areas, whereas interactive snow maps provide continuous (gap-free) coverage of the area and thus are typically validated over the whole domain. Although a considerable number of snow map validation studies were conducted in the last decade, they do not provide comprehensive information on the accuracy of satellite-derived snow maps. The principal problem is the very sparse network of meteorological stations and in situ measurements at high latitudes where snow cover is most prevalent. Therefore, reported validation results characterize the accuracy of snow cover mapping primarily in the midlatitudes. In addition, practically all validation studies have focused on North America or Eurasia. Thus, there is considerable uncertainty with respect to the accuracy of snow cover mapping in the Southern Hemisphere. It is also important to note that results of comparisons with surface observations are not sufficient to make a justified conclusion on the comparative accuracy of different automated snow products derived from satellite optical measurements. The problem is that this approach does not provide any information on the accuracy of cloud identification. Algorithms utilizing a more conservative approach for the identification of clear-sky scenes tend to overestimate the cloud cover and are more likely to provide a higher accuracy in the mapped snow cover distribution. However, this approach also results in larger cloud gaps and thus provides information on the snow cover distribution over a smaller area than snow products derived with a less conservative clear-scene identification approach.

15.3 SNOW MAPPING WITH MICROWAVE SATELLITE OBSERVATIONS

15.3.1 Physical Principles and Instrument Characteristics

The fundamental reason for using radiation in the MW portion of the electromagnetic (EM) spectrum for mapping snow cover is that these wavebands provide unique information (Woodhouse, 2006) that complements visible remote-sensing methods. MW radiation can penetrate clouds, allowing time-continuous monitoring of snow cover distribution. MWs can also penetrate a deeper layer of snow cover and interact with snow grains in a characteristic fashion, allowing estimation of SD and SWE parameters (in addition to SCA), which is not possible with visible imagery. Since natural MW radiation can be observed by passive sensors and artificial MW radiation can be generated and sensed by active sensors, the measurements can be made during the day or night. However, there are some disadvantages to MW

snow imaging. The longer MW wavelengths mean that large antennas (about a meter or longer) are required to achieve the spatial resolution appropriate for regional-scale studies (on the order of several kilometers). Active sensor systems such as the Synthetic Aperture Radar (SAR) instruments tend to be the heaviest, most power-consuming, and data-prolific space-borne instruments. MW sensors are also currently flown only aboard polar-orbiting satellites, which offer a much lower temporal resolution than optical sensors onboard geostationary satellites. In addition, as will be explained later, interpretation of MW imagery is often not as easy and straightforward as visible imagery.

MW radiation at wavelengths between 0.2 and 1.5 cm, or at frequencies between 160 and 20 GHz, has been shown to respond to snow cover ice grains in a characteristic fashion where the spectral emissivity and hence the brightness temperature as observed by a remote-sensing instrument decreases with increasing frequency. This characteristic spectral response is the result of the Rayleigh scattering behavior associated with snow grain sizes substantially smaller than the wavelength and its transition to Mie scattering behavior at larger grain sizes (for grain sizes comparable to the wavelength). Typical snow grains range between 0.2 and 0.5 mm in diameter for fine snow cover and 1 and 5 mm for coarse and very coarse grains. Figure 15.3 shows spectral MW measurements of snow and nonsnow materials made with a MW radiometer at 6, 10, 22, 37, and 94 GHz with a vertical polarization. All the listed snow types display a monotonic decrease in surface emissivity with increasing frequency, except for snow type 17 (bottom crust) at 94 and 37 GHz frequencies. The anomalous spectral response of snow type 17 (higher emissivity at 94 GHz than at 37 GHz) is explained by increased absorption (due to the presence of an ice layer)

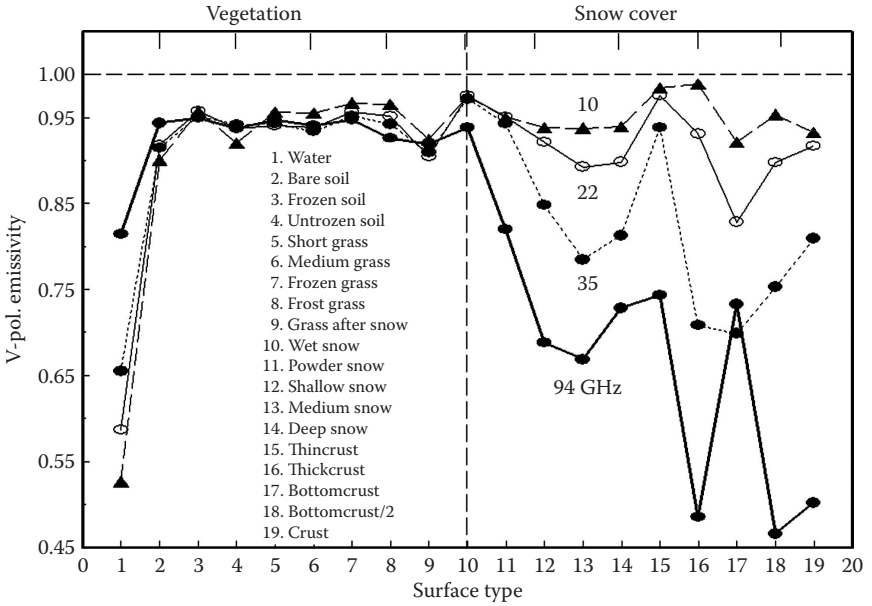

FIGURE 15.3 Spectral emissivity of snow cover and other surfaces at 10, 22, 35, and 94 GHz. (From Mätzler, C., *Meteor. Atmosph. Phys.,* 54(1–4), 241, 1994.)

TABLE 15.1
Snow Parameters That Affect Visible, Near-IR, IR, and MW Spectral Response

	Visible Solar Albedo	Near-IR Solar Albedo	Thermal IR Emissivity	MW Emissivity
Grain size	(+)	Yes		Yes
Zenith (or nadir) angle	(+)	Yes	Yes	Yes
Depth	Yes			Yes
Contaminants	Yes			
Liquid water content				Yes
Density				Yes
Temperature				Yes

+ Only if snowpack is thin or impurities are present.

or reduced scattering (due to the geometric optics limit for very large grain sizes) at higher frequencies. In contrast, water surfaces show an increase in emissivity with increasing frequency, which is typical of absorbing surfaces, whereas bare soils and vegetation show relatively small variations in emissivity with frequency.

Of particular importance for the retrieval of snow parameters is the observation that the MW spectral response shows dependence on a larger set of snow parameters than optical imagery (Table 15.1), which complicates the interpretation of MW imagery for snow identification and mapping. Among the snow parameters affecting the MW response, the most important are grain size, SD, SWE, and liquid water content. Dense vegetation can also attenuate MW radiation, particularly at higher frequencies (20 GHz and above), reducing the signal of the snow underneath. All other parameters being equal, an increase in SD or SWE is associated with a steeper emissivity gradient with frequency, because of increased scattering caused by a larger number of snow grains. Also, coarser-grained snow cover produces a steeper emissivity gradient. A small amount of liquid water in snow dramatically increases emission and reduces the scattering response and thus the ability to accurately map SCA, SD, and SWE over melting snow cover.

Table 15.2 lists the primary satellite passive MW sensors that are used for global mapping of snow cover properties, along with each instrument's average spatial resolution or the instantaneous field of view (IFOV). As shown, passive MW sensors have a coarse spatial resolution compared to optical sensors. This limits the utility of MW remote-sensing imagery for local-scale mapping of snow because smaller landscape features cannot be spatially resolved.

The earliest MW instrument used to generate snow maps is the Scanning Multichannel MW Radiometer (SMMR), flown on the Nimbus-7 Earth satellites and launched in 1978, followed by the Special Sensor MW/Imager (SSM/I) sensor on the U.S. Defense Meteorological Satellite Program (DMSP) satellites launched in 1987. The SMMR was an imaging dual polarized five-frequency radiometer (6, 10, 18, 21, and 37 GHz), while the SSM/I collects data at four frequencies (19, 22, 37,

TABLE 15.2
Main MW Sensors Used for Snow Mapping and Associated Data Characteristics

Overview of Passive MW Satellite Instruments	Mission	Availability	IFOV[a]	Comments
SMMR	Nimbus	25 Oct. 1978–20 Aug. 1987	18–27 km	
SSM/I	DMSP	July 1987–present	40–60 km	
SSMI/S	DMSP	18 Oct. 2003–present	31–4 km	Replaces SSM/I
AMSR	ADEOS-II	2003–present	20–30 km	
AMSR-E	EOS Aqua	4 May 2002–4 Oct. 2011	8–14 km	Modified from AMSR
AMSR2	GCOM-W	Planned		Future JAXA mission
AMSU	NOAA-N series METOP-A	NOAA-N series since 1998, METOP-A since 2004	48–72 km	

[a] Sizes at the instrument window channel frequency that occurs in the 30–40 GHz range, which is most frequently used for the retrieval of SD or SWE.

and 85 GHz). On the SSM/I, both vertical and horizontal polarizations are measured except at 22 GHz, for which only the vertical polarization is measured. More recent instruments include the Advanced MW Scanning Radiometer on the Earth Observing System (AMSR-E) flown on the NASA Aqua satellite, the Advanced MW Sounding Unit (AMSU) flown on the NOAA-N series and on the Meteorological Operational Satellite Programme (METOP-A), and the SSMI/S flown on DMSP. The AMSR-E is an imaging dual polarized six-frequency radiometer (6, 10, 18, 22, 37, and 89 GHz) with improved spectral and spatial resolution compared to SMMR. The AMSU contains both imaging and sounding channels in the 20–180 GHz frequency range. The sounding channels in the oxygen and water vapor absorption bands allow improved retrieval of important atmospheric parameters such as frozen precipitation (Kongoli et al., 2003). However, the AMSU lacks polarization information at the imaging channels that are useful for improved snow identification and especially snowmelt mapping. The SSMI/S instrument is a hybrid configuration between SSM/I and AMSU, containing both the SSM/I imaging and AMSU sounding channels.

15.3.2 Primary Microwave-Based Products

Most SCA retrieval algorithms from passive MW sensors are based on a decision-tree classification approach. A widely used algorithm is one developed by Grody (1991) and Grody and Basist (1996). Scattering surfaces (e.g., snow, deserts, rain, and frozen ground) and nonscattering surfaces (e.g., vegetation, bare soil, and water) are separated using brightness temperature-based scattering indices, followed by the

application of additional brightness temperature-based thresholds to remove confounding factors (e.g., rain, frozen ground, and cold deserts). The algorithm was first applied to SMMR and SSM/I observations and later adopted for application to the AMSU (Grody et al., 2000; Kongoli et al., 2005, 2007).

A variety of SD and SWE algorithms exist, including static empirical (Künzi et al., 1982; Chang et al., 1987; Goodison, 1989; Kongoli et al., 2005, 2007), dynamic empirical (Josberger and Mognard, 2002; Foster et al., 2005), dynamic semiempirical (Kelly et al., 2003), and dynamic radiative transfer inversion (Pulliainen and Hallikainen, 2001) approaches. Empirical algorithms are simple linear regression functions that typically relate the difference in measured brightness temperature at two lower-frequency atmospheric window channels (i.e., 19 and 37 GHz for the SMMR, SSM/I, and AMSR-E, and 23 and 31 GHz for the AMSU instrument) to variations in measured SD or SWE. The static algorithms apply one set of regression coefficients, whereas the dynamic ones apply seasonally and spatially adjusted coefficients. Dynamic semiempirical algorithms use simple analytical expressions of SWE as a function of satellite brightness temperature derived from radiative transfer models and temporally and spatially varying snow parameters of grain size and snow density. The physically based algorithms use nonlinear iterative inversion techniques and radiative transfer snow emission models (Mätzler and Wiesman, 1999; Pulliainen et al., 1999; Wiesmann and Mätzler, 1999).

The longest time series of MW observations used for deriving snow cover data sets is a 30 year record of combined SMMR and SSM/I daily brightness temperature data starting from 1978, and available as a 25 km Equal Area Scalable Earth (EASE)-grid at NSIDC. Based on these data, Armstrong et al. (2007) have developed a 30 year global SWE and SCA climatology that is available at NSIDC. The algorithms to derive SCA are based on the Grody and Basist (1996) methodology, and the algorithms to derive SWE are based on the Chang et al. (1987) static empirical approach. Kelly et al. (2004b) also applied the Chang et al. (1987) method to AMSR-E data to develop daily, pentad, and monthly SWE products that are also available at NSIDC. The Canadian National Snow Information System for Water (NSISW), within the framework of "State of the Canadian Cryosphere" (SOCC, see www.socc.ca), applied a regionally adjusted static SWE algorithm (Goodison, 1989) to SMMR, SSM/I, and AMSR-E observations to develop SWE climatologies for the Canadian Prairies region from 1978 to present.

The utility of MW observations for the analysis of seasonal and interannual snow cover trends and variability has been demonstrated in several studies. Tedesco et al. (2009) applied a snowmelt detection algorithm to SMRR and SSM/I data over the 1978–2008 period to study pan-arctic terrestrial snowmelt trends and possible correlations with the Arctic Oscillation (AO). Melting was detected using a spatially and temporally dynamic algorithm based on the difference between daytime and nighttime brightness temperature values. Results over the 20 year period indicated statistically significant negative trends for melt onset and end dates (0.5 and 1 days/year earlier, respectively), as well as for the length of the melt season (0.6 day/year shorter). Results indicate that the AO index variability can explain up to 50% of the melt onset variability over Eurasia and only 10% over North America, which is consistent with spatial patterns of AO-related surface temperature changes.

Brodzik et al. (2006) investigated the extent and variability in SCA using a time series of visible and MW data starting from 1978 and found a decreasing trend in the Northern Hemisphere SCA from both methods. The strongest seasonal signal occurred from May to August, when both data sets indicated significant decreasing trends. The authors suggest that this pattern was physically related to increasing air temperatures during the period of maximum seasonal snowmelt over much of the Northern Hemisphere.

Che et al. (2008) conducted a study on the spatial and temporal distribution of seasonal SD derived from passive MW satellite remote-sensing data (SMMR from 1978 to 1987 and SSM/I from 1987 to 2006) in China using Grody and Basist's (1996) methodology to identify snow cover and a modified Chang et al. (1987) algorithm to compute SD. The algorithms were first validated with meteorological observations, considering the influences from vegetation, wet snow, precipitation, cold desert, and frozen ground. The modified SD algorithm was also dynamically adjusted based on the seasonal variation of grain size and snow density. The time series of SD estimates showed that the interannual SD variation was very significant, but the SCA of seasonal snow cover in the Northern Hemisphere exhibited a weak decrease over the same period with no clear trend in SCA change in China. However, SD over the Qinghai–Tibetan Plateau and northwestern China increased, while it weakly decreased in northeastern China. Overall, SD in China during the past three decades showed significant interannual variation with a weak increasing trend.

15.3.3 Validation of Microwave Products

Similar to optical imagery, the most widely used technique for validation of MW snow products is direct comparison with collocated SD or SWE surface observations. Accuracy assessment of SCA is also made with respect to optical imagery since the latter is considered more accurate and is available at higher resolution.

The mismatch of scale between point-based surface observations and the coarse satellite footprint of available passive MW satellite sensors is a recognized problem for SWE and SD algorithm calibration and validation. Validation of SWE is even more problematic due to the fact that the abundance and reliability of good quality in situ SWE data are less than those of SD (see, e.g., Kelly et al., 2004a). Studies suggest that the sampling density of "ground truth" in situ stations footprint-matched to the satellite sensor resolution has a substantial effect on algorithm error statistics. In a large-scale validation study, Dong et al. (2005) assessed this effect by calculating error statistics of a dynamic semiempirical algorithm as a function of the number of stations matched to the 0.5° by 0.5° SSMR footprint. The mean bias errors showed improvement from more than 40 mm SWE underestimation for pixels with only one station to <30 mm SWE underestimation for pixels with five or more stations, and the corresponding mean standard deviations decreased from 80 to 45 mm (Figure 15.4). It was suggested that the most likely reason for this improvement was that the increased number of stations yields an areal average estimate that is more compatible with the remote sensor. Chang et al. (2005) report that a density of 10 ground measurements in an SSM/I or AMSR-E footprint pixel is necessary to produce a sampling error of 5 cm SD or better.

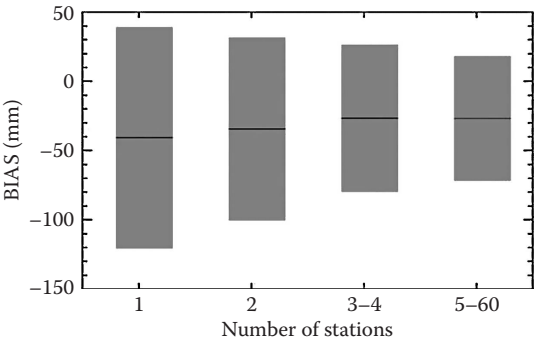

FIGURE 15.4 SWE error statistics (bias and standard deviation) as a function of the number of stations within the sensor estimate footprint. (From Dong, J. et al., *Remote Sens. Environ.,* 97(1), 68, 2005.)

Despite these issues, numerous validation studies have been conducted over the last 30 years to assess the accuracy of various MW-derived snow products, with the following results. SCA algorithms from passive MW sensors have demonstrated the ability to capture interannual and seasonal snow cover trends and variability (Armstrong and Brodzik, 2001), but regional and seasonal biases still exist. Negative biases occur for early-season shallow, melting, and forested snow covers. Positive biases occur for cold deserts, mainly attributed to desert soils scattering MW radiation similar to snow. Figure 15.5 shows maps of MW-derived SWE blended with the IMS-derived SCA taken as "ground truth" reference (maps a and c) and overlays of MW- and IMS-derived SCA (maps b and d) (Kongoli et al., 2007). Blue areas on maps b and d depict coincident SCAs, green areas depict missing MW-derived SCA, and brown areas depict false MW-derived SCA. Note the reduced extent of green areas in midwinter (map d) compared to early winter (map b), which is attributed to improved MW detection of aged, deeper snow covers. The brown areas over the Mongolian deserts are persistent and represent false MW-detected snow cover, attributed mainly to the scattering behavior of desert soils (Kongoli et al., 2007).

With respect to SWE, all passive MW products substantially underestimate wet snow, deeper snow (40 cm or greater), and snow under heavily forested terrain. As noted earlier, wet snow conditions reduce the MW scattering signal, which constitutes a fundamental physical limitation for mapping SWE over melting snow. Underestimation over deeper snow cover has been attributed to signal saturation at MW frequencies used for retrieval (Kongoli et al., 2007; Derksen, 2008), and over forest-covered snow because of the masking effect of forest canopy above the snow at frequencies of 20 GHz and above. Derksen et al. (2003) found that under these conditions, accuracy against in situ data and the ability to capture interannual variability weakened appreciably.

15.3.4 Data Assimilation Approaches for Estimating Snow Water Equivalent

Validation studies indicate that the MW-based SWE algorithms are not sufficiently accurate for operational applications. Data assimilation offers an opportunity to

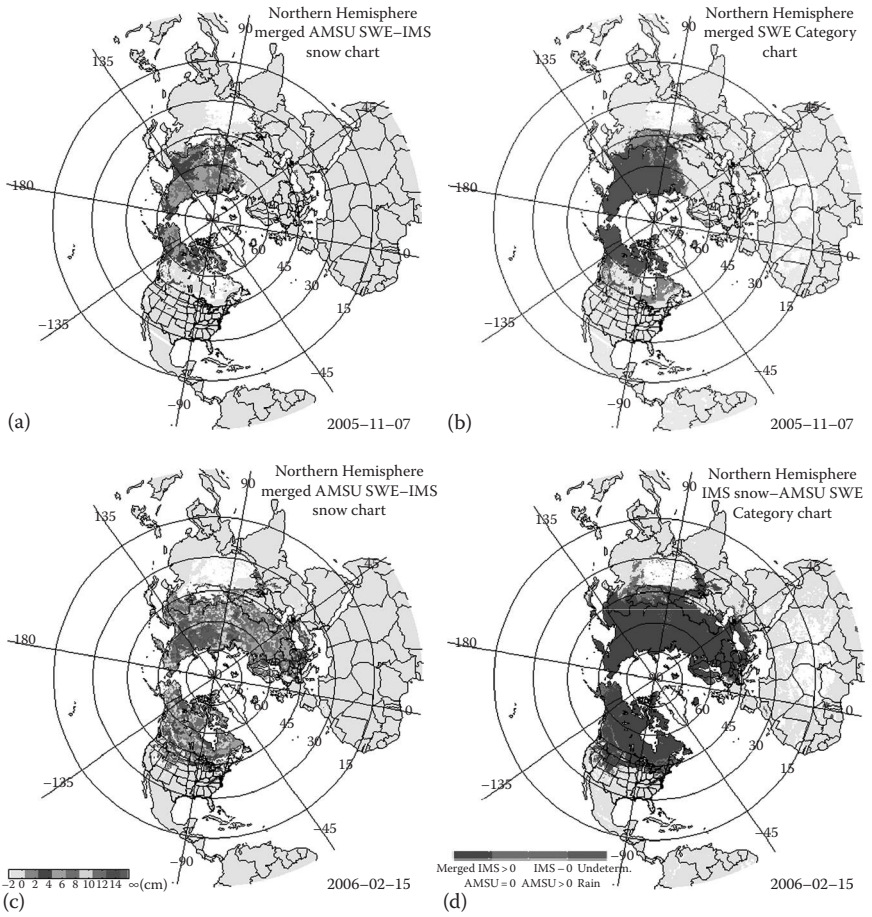

FIGURE 15.5 (See color insert.) Intercomparisons between MW-derived and IMS snow charts. (From Kongoli, C. et al., *Hydrol. Process.,* 21, 1597, 2007.) Maps a and c depict the MW-derived SWE blended with IMS-derived SCA for early and midwinter, respectively, and maps b and d depict SCA overlays of IMS and MW-derived products for early and midwinter, respectively. The SCA overlay maps (b and d) show coincident MW- and IMS-derived SCA in blue, MW-underestimated areas in green, and MW-overestimated SCA in brown (as compared to IMS taken as ground truth reference).

improve the performance of these algorithms by optimally merging information from remotely sensed and in situ observations or hydrologic model predictions.

A Bayesian assimilation technique (Pulliainen, 2006) was developed that weighs the space-borne MW data and SD interpolated from synoptic, near-real-time in situ observations with their estimated statistical accuracy. MW brightness temperature values were simulated using the Helsinki University of Technology (HUT) MW snow emission model (Pulliainen et al., 1999). The results obtained using SSM/I and AMSR-E data for northern Eurasia and Finland indicated that the employment of space-borne data using this assimilation technique improved SD and SWE retrieval accuracy (in 62% of the 3330 cases investigated) when compared with values interpolated from

in situ observations. Another large-scale study of 26,063 samples by Loujus et al. (2010) reported preliminary results from this assimilation approach that were superior to those from static empirical algorithms of Chang et al. (1987). Root mean square error (RMSE) in SWE was 43 mm for Eurasia, compared to 63–73 mm from the empirical algorithms. The RMSE was further reduced to 33.5 mm when SWE values below 150 mm were analyzed. Despite improved error statistics, the assimilation algorithm still underestimates SWE in snow deeper than 150 mm, with the bias increasing as SWE values increase.

An assimilation scheme based on an ensemble Kalman filter (EnKF) to assimilate AMSR-E brightness temperatures into the Variable Infiltration Capacity (VIC) macroscale hydrology model has also been used (Andreadis and Lettenmaier, 2005). Brightness temperature values were simulated using a Dense Media Radiative Transfer (DMRT) model (Tsang et al., 2000). The magnitude of improvement when assimilating the AMSR-E data was small and appeared mostly when the peak seasonal SWE was relatively low. For cases of increasingly deeper snowpacks, the assimilation performance degraded when compared to hydrologically modeled SWE. As a result, a maximum SWE cutoff value was incorporated, and whenever the model-predicted SWE was over a snowpack saturation value of 240 mm, the AMSR-E observation was not assimilated. On average, the results improved using this cutoff threshold, compared to results from the original run when calculations were included over high snowpack.

Dong et al. (2007) assimilated SWE estimates derived from AMSR-E data directly into a three-layer snow hydrology model (Lynch-Stieglitz, 1994) using an extended Kalman filter (EKF) and compared multiyear model simulations with and without remotely sensed SWE assimilation with in situ SWE observations. The SWE estimates from assimilation were found to be superior to both the model simulation and remotely sensed estimates alone, except when model SWE estimates were >100 mm SWE early in the snow season.

15.4 SNOW COVER MONITORING USING SYNERGY OF OPTICAL AND MICROWAVE REMOTE-SENSING TECHNIQUES

Physical limitations inherent to automated optical and MW snow remote-sensing techniques result in their inability to provide continuous and accurate snow cover information at high spatial resolution under a variety of atmospheric, physiogeographic, and climatic conditions. This substantially reduces the value of snow cover products derived from individual satellite sensors and complicates their use in numerical model applications and in climate studies. In an attempt to improve satellite-based snow cover characterization, several techniques and algorithms have been proposed to combine snow cover observations in the optical and MW spectral bands. The principal objective of these techniques is to maximize advantages that optical and MW observations offer in an effort to provide continuous areal coverage of snow cover maps at the highest possible spatial and temporal resolution with the highest possible accuracy.

Armstrong et al. (2003) combined MODIS-based 8 day composited SCA maps with 8 day SWE maps derived from SSM/I data to produce an 8 day blended, 25 km resolution global SCA map. The technique integrated snow identified from the optical MODIS data with snow information from SSM/I to compensate for

possible omissions of shallow or melting snow in the MW-based snow product. Foster et al. (2010) used the daily 5 km MODIS SCA product and the 25 km AMSR-E SWE retrievals to generate a daily blended SCA map. Because optical snow retrievals provide better accuracy and spatial resolution than the MW-based retrievals, the algorithm relies on MODIS data if available. Pixels that were cloud covered or did not have enough daylight to perform classification with MODIS data are filled in with AMSR-E retrievals. As a result, the output product presents a global binary (snow/no snow) 25 km map with no cloud-related coverage gaps. A similar approach to blending of MODIS and AMSR-E products has been used by Liang et al. (2008) to characterize daily changes of snow cover distribution over China.

A blending technique by Romanov et al. (2000) presents a more cautious approach to the use of MW-based snow retrievals from satellite observations. The algorithm combines observations from GOES Imager instruments onboard the GOES-East and GOES-West satellites with observations from SSM/I. Optical retrievals from the GOES imagers are used as the primary data source for the blended map, and MW data are added if the area was identified as "cloudy" by GOES. The principal difference of this approach from the one of Foster et al. (2010) is that MW observations classified as "snow-free land surface" are disregarded in the blending technique because of frequent omission of melting snow and shallow snow in the MW product. MW snow retrievals over mountains are also disregarded because of their tendency to confuse cold rocky surfaces with snow and thus to overestimate snow cover extent in high-altitude areas. At the final processing stage, pixels that remain "undetermined" in the current-day snow map are filled in with the data from the previous day's blended snow map. In 2000, this blending algorithm was implemented operationally at NOAA/NESDIS to generate 4 km daily snow maps over North America. In 2006, this snow-mapping system was upgraded by adding optical observations from NOAA AVHRR and MSG SEVIRI. The latter allowed the snow-mapping domain to be expanded from North America to the whole globe.

Since the blended snow cover map comprises both optical and MW snow retrievals, its overall accuracy typically ranges within the accuracy of the contributing products. In the cloud-clear portions of the imagery, the accuracy of the blended product and its effective spatial resolution is identical to the accuracy and spatial resolution of the optical SCA map. In cloudy areas, both the effective spatial resolution and the accuracy of the blended product degrade to the level corresponding to MW retrievals. The principal benefit of the blended product over the optical-based SCA maps is in its continuous area coverage, while providing a higher classification accuracy and better spatial resolution over clear-sky areas compared to MW-based products.

15.5 APPLICATION OF SATELLITE-BASED SNOW PRODUCTS FOR DROUGHT IDENTIFICATION AND MONITORING

The example provided in this section demonstrates a possible application of satellite-derived SCA maps to assess the spring snowmelt water availability and hence to facilitate the prediction of early-spring drought conditions. Note that a better assessment of spring snowmelt can be made by accurate knowledge of the SWE distribution before the onset of spring snowmelt, which would require application

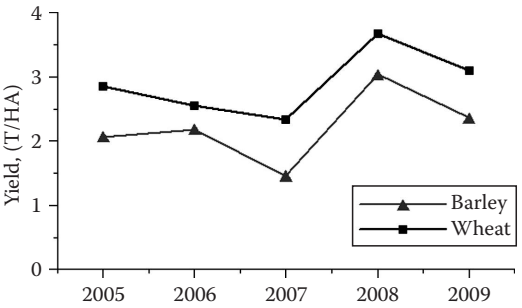

FIGURE 15.6 Yearly yield of barley and wheat in Ukraine, 2005–2009. Data were obtained from the USDA FAS Production, Supply and Distribution data set (online at http://www.fas.usda.gov/psdonline/psdQuery.aspx).

of satellite-derived SWE maps (not included in this section). However, as validation studies presented earlier have shown, the reliability of the available satellite-based operational SWE products for such assessments is questionable at this current time.

The case study is focused on Ukraine, which is one of the world's largest grain exporters of winter crops (primarily wheat and barley) that account for most of the country's total annual grain production. Snow cover plays an important role in winter crop production in Ukraine. The duration of the snow season ranges from several weeks in the southernmost part of the country to several months in the north. In addition to providing the source of snowmelt water for winter crop development in early spring, the snowpack also prevents these crops from frost and freeze damage during the winter. In spring 2007, a severe drought occurred in Ukraine, which seriously affected winter grain production. According to the data of USDA's Foreign Agricultural Service (FAS), in 2007, winter barley and wheat yields were approximately 10% and 30% less than in 2006 and 35% and 50% less than in 2008 (Figure 15.6). In an attempt to gain better insight into the origin of the drought and its possible relationship to the snow cover properties, we calculated and examined seasonal variations of the snow cover distribution in Ukraine. NOAA's IMS daily interactive snow cover maps were used to generate maps of snow cover duration for 10 consecutive winter seasons from 2000–2001 to 2008–2009. For every grid cell of the map, the duration of winter snow cover was estimated by calculating the number of days with snow cover within an annual snow season time period starting on August 1 and ending July 31 of the next year. The IMS product was applied in this study since NESDIS blended snow cover maps were not available before 2006.

Figure 15.7 presents IMS-derived estimates of the duration of snow cover in Ukraine during the 2006–2007 winter season as well as for two preceding and subsequent winters. As shown, the 2006–2007 winter season was characterized by substantially shorter duration of snow cover. Compared to the mean snow cover duration calculated for 10 winter seasons (2000–2009), in 2006–2007 the snow cover stayed on the ground 40–50 days less in the northern part of the country and about 20 days less in the south. In Ukraine, as well as in other midlatitude regions that are characterized by a persistent winter snow cover, SWE tends to gradually increase throughout the winter season. As a result, shorter (longer) snow cover duration results in a smaller (larger) amount

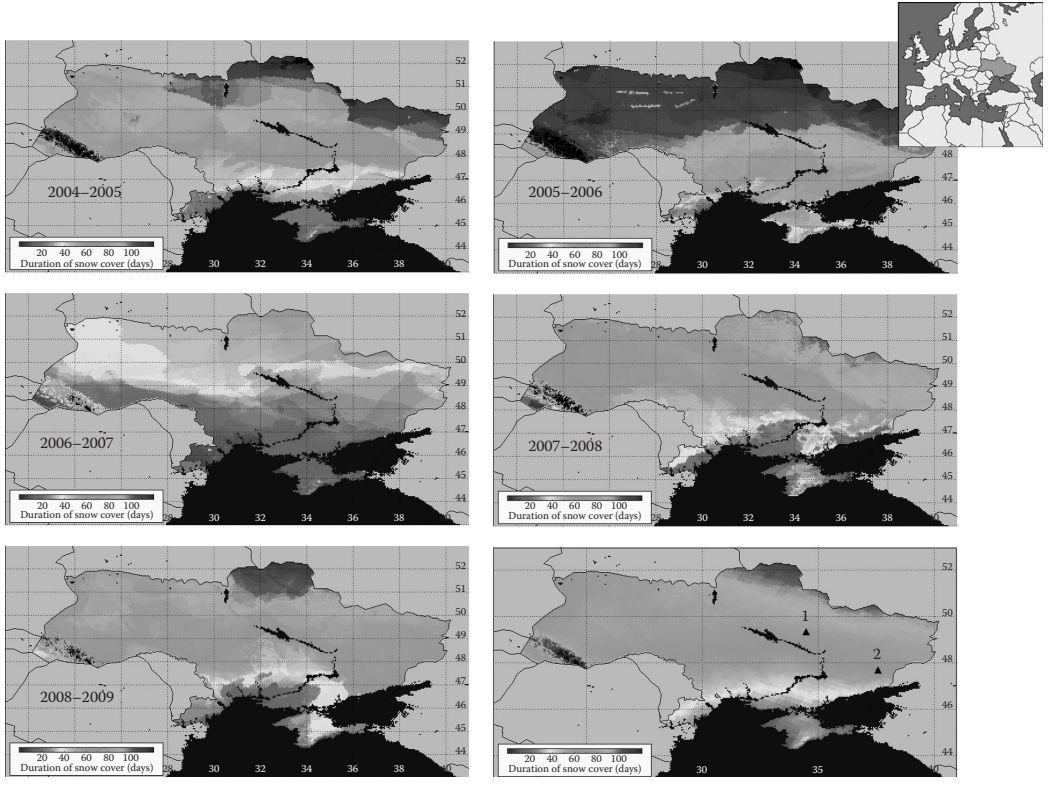

FIGURE 15.7 **(See color insert.)** Maps of seasonal snow cover duration over Ukraine for selected years and the mean seasonal snow cover duration for the years 2000–2009. The upper right image shows the location of Ukraine in Europe. Triangles in the map of the mean duration of snow cover (in the lower right) indicate the location of Poltava (1) and Donetsk (2).

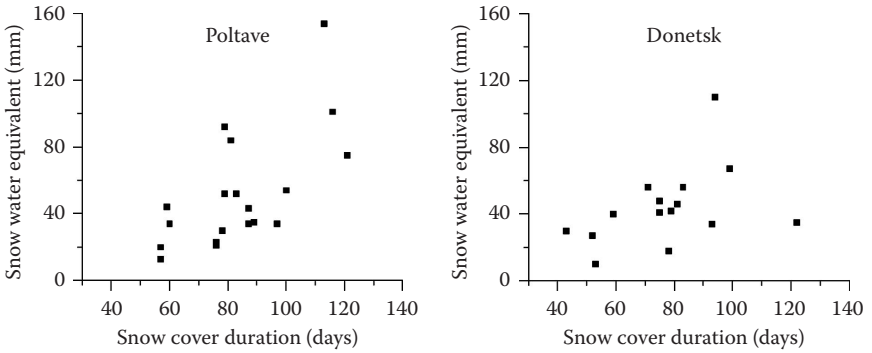

FIGURE 15.8 Scatter plots of snow cover duration and maximum SWE observed during a month-long period preceding the snowmelt for two locations in Ukraine: Poltava (49.36°N, 34.33°E) and Donetsk (48.04°N, 37.46°E). The location of the two stations is shown in Figure 15.7. The results are presented for the years 1967–1990. Snow cover duration and SWE data at the two stations were acquired from the Former Soviet Union Hydrological Snow Surveys data set available at NSIDC. (From Krenke, A., *Former Soviet Union Hydrological Snow Surveys, 1966–1996*, National Snow and Ice Data Center/World Data Center for Glaciology, Digital media, Boulder, CO, 1998.)

of water accumulated in the snowpack and released during the spring snowmelt, and, thus, snow duration can be used as a proxy for SWE available for spring snowmelt.

Figure 15.8 presents the statistics on the snow cover duration and the maximum seasonal SWE observed in Poltava (49.36°N, 34.33°E) and Donetsk (48.04°N, 37.46°E). The location of these stations is shown in Figure 15.7. These in situ observations were acquired from the Former Soviet Union Hydrological Snow Surveys data set available at NSIDC (Krenke, 1998) and cover the time period from 1967 to 1990. Both graphs in Figure 15.8 clearly demonstrate a decreasing trend in SWE by the end of the winter season with the decreasing duration of the seasonal snow cover. The analysis of IMS-derived maps of snow duration revealed that in the winter of 2006–2007 the duration of snow cover in Poltava and Donetsk was about three times less than normal and comprised 32 and 26 days, respectively. This anomalously short duration of the snow season gives a clear indication that the amount of moisture accumulated in the snowpack by the end of winter was also anomalously low. The shorter snow cover duration of the 2006–2007 winter season and the associated decline in snowmelt water may have contributed to the shortage of soil moisture for plant development in the spring and to drought conditions that occurred in early summer 2007. The early spring period spans the critical vegetative and reproductive growth stages of both winter wheat and barley that determine the final grain yield. Lower amounts of available soil moisture at the beginning of the 2007 growing season due to less spring snowmelt compared to the adjacent years are supported by soil moisture data derived from AMSR-E observations (Figure 15.9). Monthly soil moisture maps were generated from corresponding daily AMSR-E-based maps (AE_Land3 product) available at NSIDC (http://nsidc.org/data/ae_land3.html). As shown in Figure 15.9, the monthly average soil moisture values in the early spring months (March, April, and May) were noticeably lower in 2007 than in 2006. The largest soil moisture deficit in 2007 occurred in the central and eastern part of the country where most winter barley

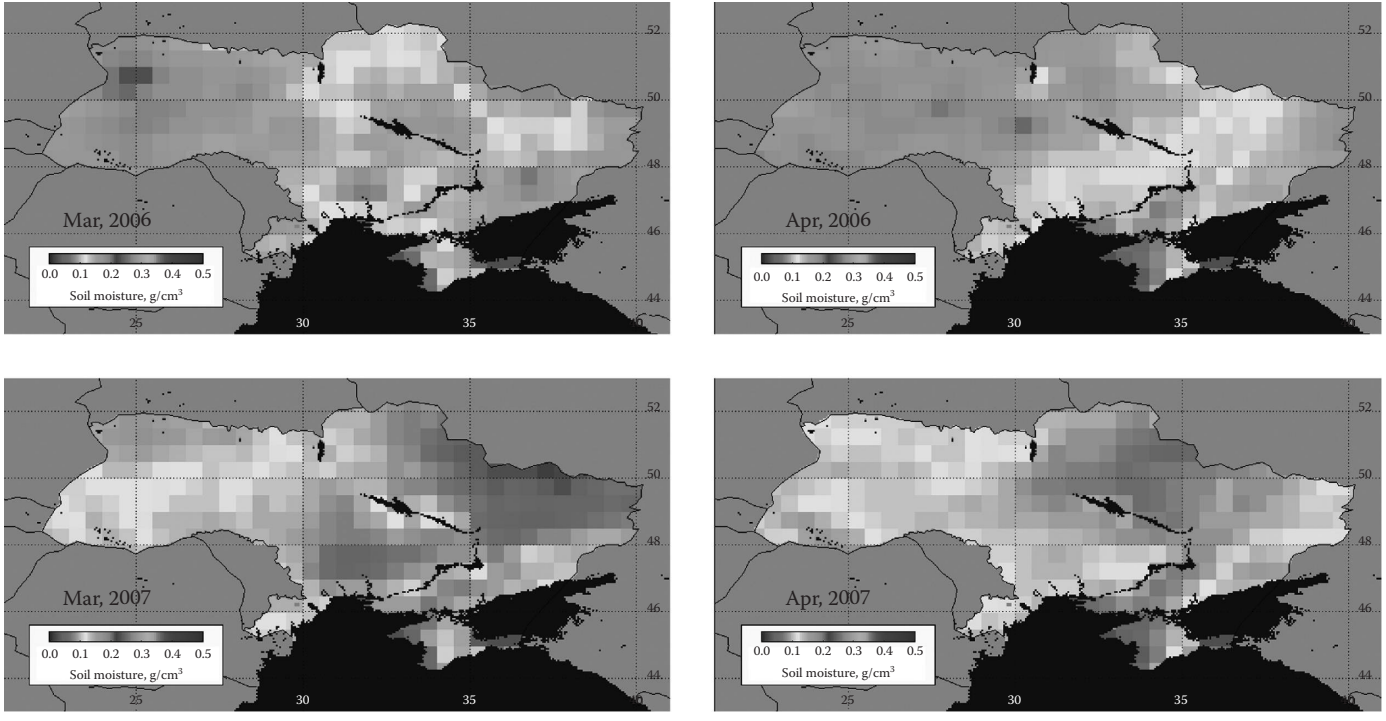

FIGURE 15.9 **(See color insert.)** Monthly average soil moisture over Ukraine for the months of March and April of 2006 and 2007. Soil moisture was retrieved from AMSR-E Aqua data.

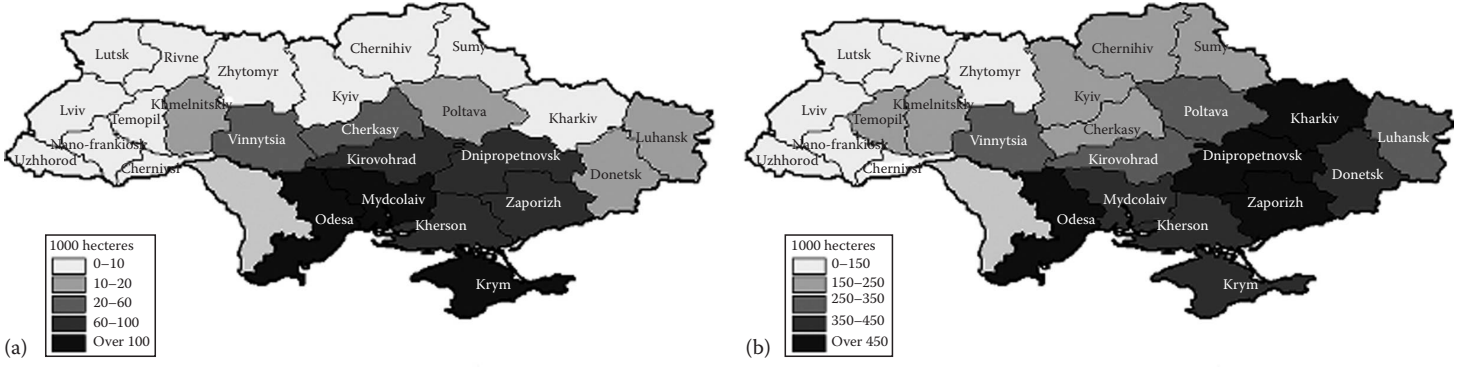

FIGURE 15.10 Area of winter barley (a) and winter wheat (b) in Ukraine (USDA FAS data).

and wheat are grown (see Figure 15.10). Lower levels of soil moisture in spring 2007 have also been confirmed by in situ measurements. In particular, according to reports from Poltava and Donetsk stations, the soil moisture in the top 20 cm of soil at the end of March 2007 was about 20% less than normal for these locations for this time of the year.

Although spring snowmelt presents an important source of moisture for crops at the beginning of the growing season, snow cover is by no means the only factor that has to be accounted for in winter crop condition monitoring and yield forecasting. Short duration of seasonal snow cover should be viewed only as indirect evidence of reduced winter precipitation that may contribute to the development of drought conditions later in spring. Other factors, such as soil moisture and precipitation in the preceding fall season and, most notably, the amount of liquid precipitation in early spring, also affect availability of soil moisture for crop development at the beginning of the growth season. As a result, snow cover products should be used in combination with other data sources reflecting other environmental conditions (e.g., precipitation, soil moisture, and vegetation health) to develop a more complete picture of early growing season drought conditions in the spring. A more detailed analysis of precipitation in Ukraine in winter 2006–2007 and spring 2007 has shown that the lack of water from snowmelt was not the only factor that caused drought conditions in 2007. Substantially lower amounts of precipitation were observed over most of the country later into the growing season, in March, April, and May. Time series of monthly precipitation amounts for two locations in Ukraine (see Figure 15.11)

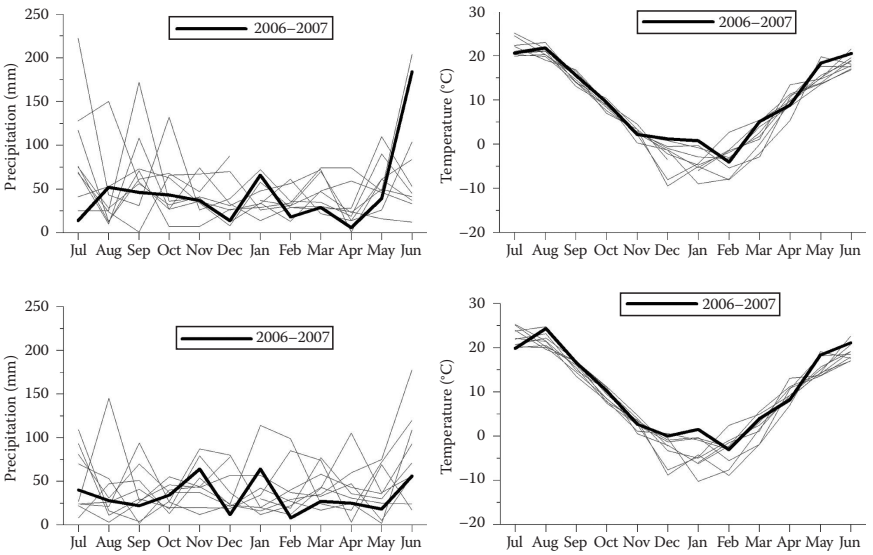

FIGURE 15.11 Seasonal time series of the monthly total precipitation and monthly mean air temperature at two stations in Ukraine, Poltava (upper row) and Donetsk (lower row), for the years 2000–2009. Precipitation and air temperature for the period from August 2006 to July 2007 are shown in black; data for all other years are shown in gray. Values of monthly total precipitation and monthly mean temperature were acquired from NCDC.

clearly demonstrate less than average precipitation amounts in December 2006 and in February–April 2007. Precipitation in January 2007 was somewhat higher than average, but apparently it was not sufficient to fully compensate for the precipitation shortage during the rest of the months. The time series of monthly mean temperature in Figure 15.11 show that the winter season of 2006–2007 was unusually warm. The mean temperature in December and January at both locations (Poltava and Donetsk) was above the freezing level, whereas in February it decreased to several degrees below 0°C. Relatively high wintertime temperatures give a reason to believe that no or very little freeze damage to winter crops occurred in the winter of 2006–2007.

15.6 CONCLUSIONS

In this chapter, a review of principal satellite remote-sensing methods for snow monitoring was provided, with an emphasis on the mapping of hydrologically important snow parameters of SWE, SD, and SCA. Satellite observations can complement in situ measurements by providing time- and space-continuous snow cover information, facilitating more accurate snowmelt runoff forecasting and drought predictions. Validation, accuracy assessment, and limitations of current remote sensing–based snow information received special attention. Optical remote sensing–based SCA products achieve a high accuracy (exceeding 94%) over areas not heavily forested and snowpack deeper than 1 cm. Given the relatively high spatial (1–4 km) and temporal (hourly for geostationary and daily for polar-orbiting sensors) resolution of optical satellite-based instruments, they can be used successfully to derive accurate snow cover distribution information for snowmelt runoff forecasting and drought assessment for many SCA of the world. This capability was demonstrated in a case study over Ukraine. An inherent limitation of optical remote-sensing snow cover information is that it is available only during the day and over cloud-free areas. MW-based snow cover information, on the other hand, is available during both day and night and under cloudy conditions to monitor snow cover distribution. In addition, MW imagery offers the capability of mapping SD and SWE, which are more physically related to snowmelt than SCA. Overall, passive MW-derived SCA using current operational algorithms shows agreement with observed seasonal and interannual trends, and thus has the ability to provide useful complementary winter moisture information to the optical-based sources. However, seasonal biases still exist. SCA is underestimated over melting snow, early season shallow snow, and forested snow covers and overestimated in cold desert soils. In addition, underestimations of SWE and SD occur for snow cover deeper than 40 cm. In order to maximize advantages of optical and passive MW imagery, several SCA blending techniques and products were also discussed. The principal benefit of the blended satellite products over the optical-based products is that they provide continuous SCA coverage, while achieving a higher classification accuracy and better spatial resolution over clear-sky areas compared to passive MW-based products. Recent blending (assimilation) approaches that combine MW-derived SWE and in situ or modeled SWE show encouraging results and

performance superior to existing passive MW-based SWE approaches. However, none of the assimilation approaches improved performance over melting and deeper snow covers.

REFERENCES

Andreadis, K.M. and D.P. Lettenmaier. 2005. Assimilating passive microwave brightness temperature for snow water equivalent estimation. *American Meteorological Society Annual Meeting, 19th Conference on Hydrology*, San Diego, CA. Boston, MA: American Meteorological Society.

Armstrong, R.L. and M.J. Brodzik. 2001. Validation of passive microwave snow algorithms. *Remote Sensing and Hydrology 2000*, IAHS Publication No. 267:87–92.

Armstrong, R.L., M.J. Brodzik, K. Knowles, and M. Savoie. 2007. *Global Monthly EASE-Grid Snow Water Equivalent Climatology*. Boulder, CO: National Snow and Ice Data Center, Digital media.

Armstrong, R.L., M.J. Brodzik, M. Savoie, and K. Knowles. 2003. Enhanced hemispheric-scale snow mapping through the blending of optical and microwave satellite data. *Geophysical Research Abstracts* 5:12824.

Ault, T., K.P. Czajkowski, T. Benko, J. Coss, J. Struble, A. Spongberg, M. Templin, and C. Gross. 2006. Validation of the MODIS snow product and cloud mask using student and NWS cooperative station observations in the Lower Great Lakes Region. *Remote Sensing of Environment* 105:341–353.

Baum, B.A. and Q. Trepte. 1999. A grouped threshold approach for scene identification in AVHRR imagery. *Journal of Atmospheric and Oceanic Technology* 16:793–800.

Brodzik, M.J., R.L. Armstrong, E.C. Weatherhead, M.H. Savoie, K.W. Knowles, and D.A. Robinson. 2006. Regional trend analysis of satellite-derived snow extent and global temperature anomalies. American Geophysical Union Fall Meeting Supplement, *EOS Transactions* 87(52):Abstract U33A-0011.

Chang, A.T.C., J.L. Foster, and D.K. Hall. 1987. Nimbus - 7 SMMR derived global snow cover parameters. *Annals of Glaciology* 9:39–44.

Chang, A.T.C., R.E.J. Kelly, E.J. Josberger, R.L. Armstrong, and J.L. Foster. 2005. Analysis of gauge-measured and passive microwave derived snow depth variations of snowfields. *Journal of Hydrometeorology* 6:20–33.

Che, T., X. Li, R. Jin, R. Armstrong, and T. Zhang. 2008. Snow depth derived from passive microwave remote-sensing data. *Annals of Glaciology* 49:145–154.

Derksen, C. 2008. The contribution of AMSR-E 18.7 and 10.7 GHz measurements to improved boreal forest snow water equivalent retrievals. *Remote Sensing of Environment* 112:2700–2709.

Derksen, C., A. Walker, and B. Goodison. 2003. A comparison of 18 winter seasons of in situ and passive microwave-derived snow water equivalent estimates in Western Canada. *Remote Sensing of Environment* 88(3):271–282.

de Wildt, M., G. Seiz, and A. Gruen. 2007. Operational snow mapping using multitemporal Meteosat SEVIRI imagery. *Remote Sensing of Environment* 109:29–41.

Dong, J., J. Walker, P. Houser, and C. Sun. 2007. Scanning multichannel microwave radiometer snow water equivalent assimilation. *Journal of Geophysical Research* 112:D07108, doi:10.1029/2006JD007209.

Dong, J., J.P. Walker, and P.R. Houser. 2005. Factors affecting remotely sensed snow water equivalent uncertainty. *Remote Sensing of Environment* 97(1): 68–82.

Dozier, J., R.O. Green, A.W. Nolin, and T.H. Painter. 2009. Interpretation of snow properties from imaging spectrometry. *Remote Sensing of Environment* 113(1):S25–S37.

Dozier, J. and T.H. Painter. 2004. Multispectral and hyperspectral remote sensing of alpine snow properties. *Annual Review of Earth and Planetary Sciences* 32:465–494.

Fang, X. and J.W. Pomeroy. 2007. Snowmelt runoff sensitivity analysis to drought on the Canadian prairies. *Hydrological Processes* 21:2594–2609.

Fang, X. and J.W. Pomeroy. 2008. Drought impacts on Canadian prairie wetland snow hydrology. *Hydrological Processes* 22:2858–2873.

Foster, J.L., D.K. Hall, J.B. Eylander, G.A. Riggs, S.V. Nghiem, M. Tedesco, E.J. Kim, P.M. Montesano, R.E.J. Kelly, K.A. Casey and B. Choudhury. 2010. A blended global snow product using visible, passive microwave and scatterometer data. *International Journal of Remote Sensing* 32(5):1371–1395.

Foster, J.L., C.J. Sun, J.P. Walker, R. Kelly, A. Chang, J.R. Dong, and H. Powell. 2005. Quantifying the uncertainty in passive microwave snow water equivalent observations. *Remote Sensing of Environment* 94(2):187–203.

Frei, A. 2009. A new generation of satellite snow observations for large scale earth system studies. *Geography Compass* 3:879–902.

Frei, A. and D.A. Robinson. 1999. Northern Hemisphere snow extent: Regional variability 1972 to 1994. *International Journal of Climatology* 19:1535–1560.

Goodison, B.E. 1989. Determination of areal snow water equivalent on the Canadian prairies using passive microwave satellite data. *IEEE International Geoscience and Remote Sensing Symposium*, Vancouver, Canada.

Gray, D.M., J.W. Pomeroy, and R.J. Granger. 1989. Modelling snow transport, snowmelt and meltwater infiltration in open, northern regions. In *Northern Lakes and Rivers*, ed. W.C. Mackay, Occasional Publication No. 22, pp. 8–22. Edmonton, Alberta, Canada: Boreal Institute for Northern Studies, University of Alberta.

Grody, N.C. 1991. Classification of snow cover and precipitation using the special sensor microwave imager. *Journal of Geophysical Research* 96(D4):7423–7435.

Grody, N.C. and A.N. Basist. 1996. Global identification of snow cover using SSM/I measurements. *IEEE Transactions on Geoscience Remote Sensing* 34(1):237–249.

Grody, N.C., F. Weng, and R. Ferraro. 2000. Application of AMSU for obtaining hydrological parameters. In *Microwave Radiometry and Remote Sensing of the Earth's Surface and Atmosphere*, eds. P. Pampalono and S. Paloscia, pp. 339–351. Zeist, the Netherlands: Vision Sports Publishing.

Hall, D.K. and G.A. Riggs. 2007. Accuracy assessment of the MODIS snow-cover products. *Hydrological Processes* 21:1534–1547.

Hall, D.K., G.A. Riggs, V.V. Salomonson, N. DiGiromamo, and K.J. Bayr. 2002. MODIS snow-cover products. *Remote Sensing of Environment* 83:181–194.

Helfrich, S.R., D. McNamara, B.H. Ramsay, T. Baldwin, and T. Kasheta. 2007. Enhancements to, and forthcoming developments in the Interactive Multisensor Snow and Ice Mapping System (IMS). *Hydrological Processes* 21:1576–1586.

Josberger, E.G. and N.M. Mognard. 2002. A passive microwave snow depth algorithm with a proxy for snow metamorphism. *Hydrological Processes* 16(8):1557–1568.

Kelly, R.E.J., T.C. Alfred, J. Chang, J.L. Foster, and M. Tedesco. 2004b. Updated daily, 5-day and monthly. *AMSR-E/Aqua Monthly L3 Global Snow Water Equivalent EASE-Grids* V002. Boulder, CO: National Snow and Ice Data Center, Digital media.

Kelly, R.E., A.T. Chang, L. Tsang, and J.L. Foster. 2003. A prototype AMSR - E global snow area and snow depth algorithm. *IEEE Transactions on Geoscience and Remote Sensing* 41(2):230–242.

Kelly, R.E.J., N.A. Drake, and S.L. Barr. 2004a. *Spatial Modelling of the Terrestrial Environment*. Chichester, U.K.: John Wiley and Sons Ltd.

Khlopenkov, K.V. and A.P. Trishchenko. 2007. SPARC: New cloud, snow, and cloud shadow detection scheme for historical 1-km AVHRR data over Canada. *Journal of Atmospheric and Oceanic Technology* 24:322–343.

Kongoli, C., C. Dean, S. Helfrich, and R. Ferraro. 2007. Estimating the potential of a blended passive microwave-interactive multi-sensor snow water equivalent product for improved mapping of snow cover and estimations of snow water equivalent. *Hydrological Processes* 21:1597–1607.

Kongoli, C., R. Ferraro, P. Pellegrino, and H. Meng. 2005. Snow microwave products from the NOAA's Advanced Microwave Sounding Unit. *Proceedings of the 19th Conference on Hydrology,* San Diego, CA. Boston, MA: American Meteorological Society.

Kongoli, C., P. Pellegrino, R.R. Ferraro, N.C. Grody, and H. Meng. 2003. A new snowfall detection algorithm over land using measurements from the Advanced Microwave Sounding Unit (AMSU). *Geophysical Research Letters* 30(4):1756–1759.

Krenke, A. 1998. *Former Soviet Union Hydrological Snow Surveys, 1966-1996*. Edited by NSIDC. Boulder, CO: National Snow and Ice Data Center/World Data Center for Glaciology, Digital media.

Künzi, K.F., S. Patil, and H. Rott. 1982. Snow-cover parameters retrieved from Nimbus-7 Scanning Multichannel Microwave Radiometer (SMMR) data. *IEEE Transactions on Geoscience and Remote Sensing* 20(4):452–467.

Liang, T., X. Zhang, H. Xie, C. Wu, Q. Feng, X. Huang, and Q. Chen. 2008. Toward improved daily snow cover mapping with advanced combination of MODIS and AMSR-E measurements. *Remote Sensing of Environment* 112:3750–3761.

Loujus, K., J. Pulliainen, M. Takala, C. Derksen, H. Rott, T. Nagler, R. Solberg, A. Wiesmann, S. Metsamaki, E. Malnes, and B. Bojkov. 2010. Investigating the feasibility of the GLOBESNOW snow water equivalent data for climate research purposes. *Proceedings of IEEE International Geoscience and Remote Sensing Symposium*, Honolulu, HI.

Lynch-Stieglitz, M. 1994. The development and validation of a simple snow model for the GISS GCM. *Journal of Climate* 7:1842–1855.

Mätzler, C. 1994. Passive microwave signatures of landscapes in winter. *Meteorology and Atmospheric Physics* 54(1–4):241–260.

Mätzler, C. and A. Wiesmann. 1999. Extension of the microwave emission model of layered snowpacks to coarse-grained snow. *Remote Sensing of Environment* 70(3):317–325.

Pagano, T.C. and D.C. Garen. 2006. Integration of climate information and forecasts into western US water supply forecasts. In *Climate Variations, Climate Change, and Water Resources Engineering*, eds. J. D. Garbrecht and T. C. Piechota, pp. 86–103. Reston, VA: American Society of Civil Engineers.

Pulliainen, J. 2006. Mapping of snow water equivalent and snow depth in boreal and sub-arctic zones by assimilating space-borne microwave radiometer data and ground-based observations. *Remote Sensing of Environment* 101(2):257–269.

Pulliainen, J.T., J. Grandell, and M.T. Hallikainen. 1999. HUT snow emission model and its applicability to snow water equivalent retrieval. *IEEE Transactions on Geoscience and Remote Sensing* 37(3):1378–1390.

Pulliainen, J. and M. Hallikainen. 2001. Retrieval of regional snow water equivalent from space-borne passive microwave observations. *Remote Sensing of Environment* 75(1):76–85.

Ramsay, B. 1998. The interactive multisensor snow and ice mapping system. *Hydrological Processes* 12:1537–1546.

Romanov, P., G. Gutman, and I. Csiszar. 2000. Automated monitoring of snow over North America with multispectral satellite data. *Journal of Applied Meteorology* 39:1866–1880.

Romanov, P. and D. Tarpley. 2006. Monitoring snow cover over Europe with Meteosat SEVIRI. *Proceedings of the 2005 EUMETSAT Meteorological Satellite Conference*, pp. 282–287, Dubrovnik, Croatia.

Simic, A., R. Fernandes, R. Brown, P. Romanov, and W. Park. 2004. Validation of VEGETATION, MODIS, and GOES C SSM/I snow-cover products over Canada based on surface snow depth observations. *Hydrological Processes* 18(6):1089–1104.

Simpson, J.J., J.R. Stitt, and M. Sienko. 1998. Improved estimates of the areal extent of snow cover from AVHRR data. *Journal of Hydrology* 204:1–23.

Tedesco, M., M. Brodzik, R. Armstrong, M. Savoie, and J. Ramage. 2009. Pan arctic terrestrial snowmelt trends (1979-2008) from spaceborne passive microwave data and correlation with the Arctic Oscillation. *Geophysical Research Letters* 36:L21402, doi:10.1029/2009GL039672.

Tsang, L., C. Chen, A.T.C. Chang, J. Guo, and K. Ding. 2000. Dense media radiative transfer theory based on quasicrystalline approximation with applications to passive microwave remote sensing of snow. *Radio Science* 35(3):731–749.

Wheaton E., V. Wittrock, S. Kulshreshtha, G. Koshida, C. Grant, A. Chipanshi, and B. Bonsal. 2005. Lessons learned from the Canadian drought years 2001 and 2002: Synthesis report. Publication No. 11602-46E0. Prepared for Agriculture and Agri-Food Canada, SRC, Saskatoon, Saskatchewan.

Wiesmann, A. and C. Mätzler. 1999. Microwave emission model of layered snowpacks. *Remote Sensing of Environment* 70(3):307–316.

Wiscombe, W.J. and S.G. Warren. 1980. A model for the spectral albedo of snow. Part I: Pure snow. *Journal of the Atmospheric Sciences* 37:2712–2733.

Woodhouse, I. 2006. *Introduction to Microwave Remote Sensing*. Boca Raton, FL: CRC Press.

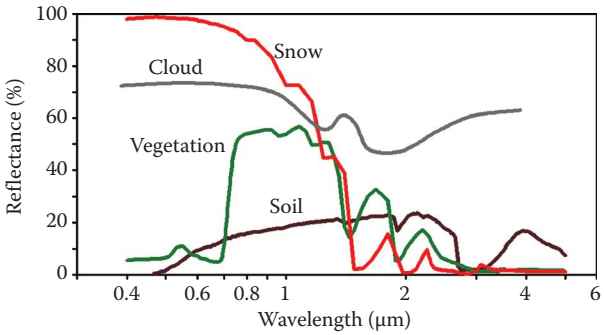

FIGURE 15.2 Spectral reflectance for different land surface cover types including snow.

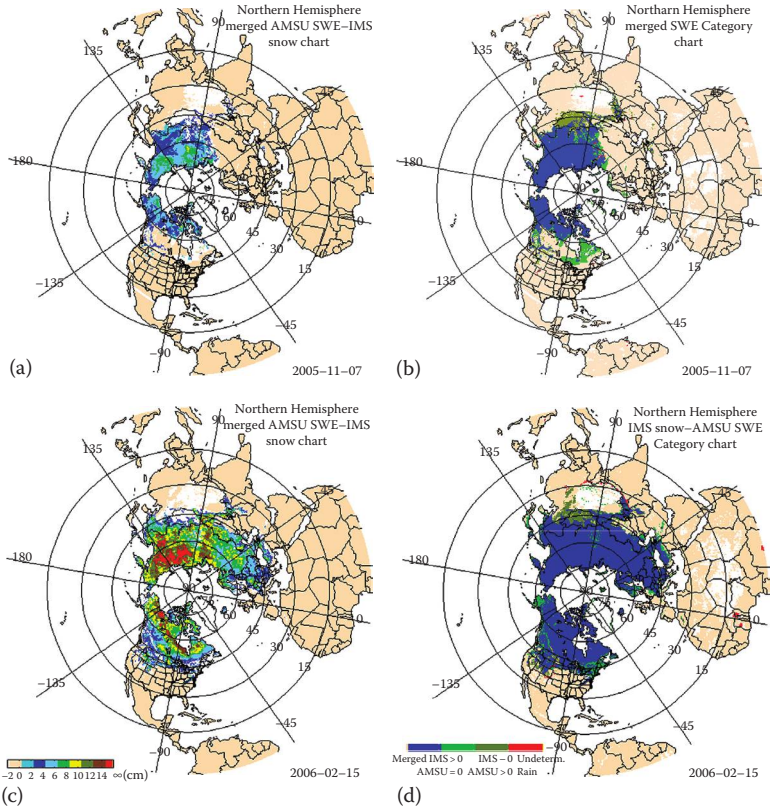

FIGURE 15.5 Intercomparisons between MW-derived and IMS snow charts. (From Kongoli, C. et al., *Hydrol. Process.,* 21, 1597, 2007.) Maps a and c depict the MW-derived SWE blended with IMS-derived SCA for early and midwinter, respectively, and maps b and d depict SCA overlays of IMS and MW-derived products for early and midwinter, respectively. The SCA overlay maps (b and d) show coincident MW- and IMS-derived SCA in blue, MW-underestimated areas in green, and MW-overestimated SCA in brown (as compared to IMS taken as ground truth reference).

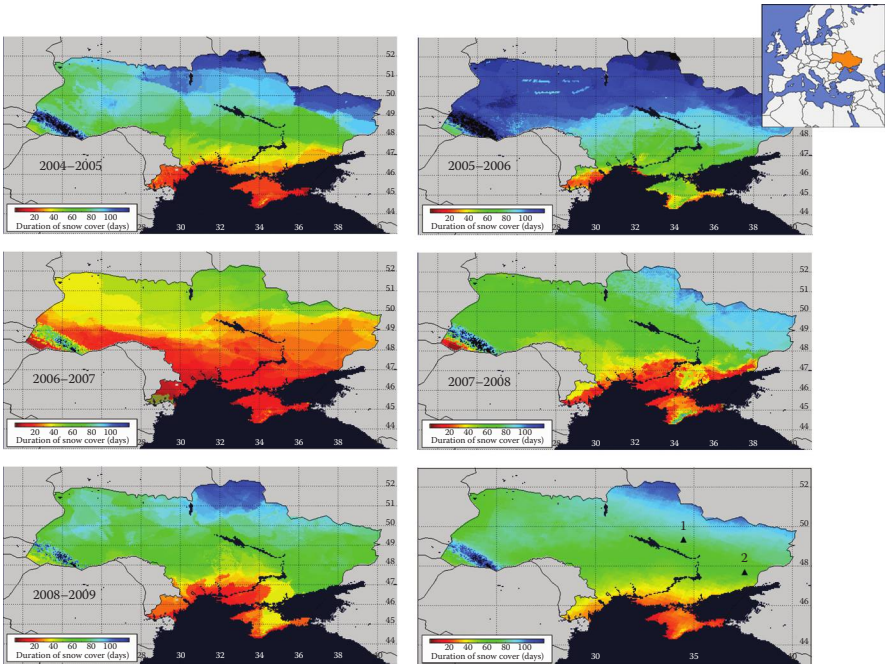

FIGURE 15.7 Maps of seasonal snow cover duration over Ukraine for selected years and the mean seasonal snow cover duration for the years 2000–2009. The upper right image shows the location of Ukraine in Europe. Triangles in the map of the mean duration of snow cover (in the lower right) indicate the location of Poltava (1) and Donetsk (2).

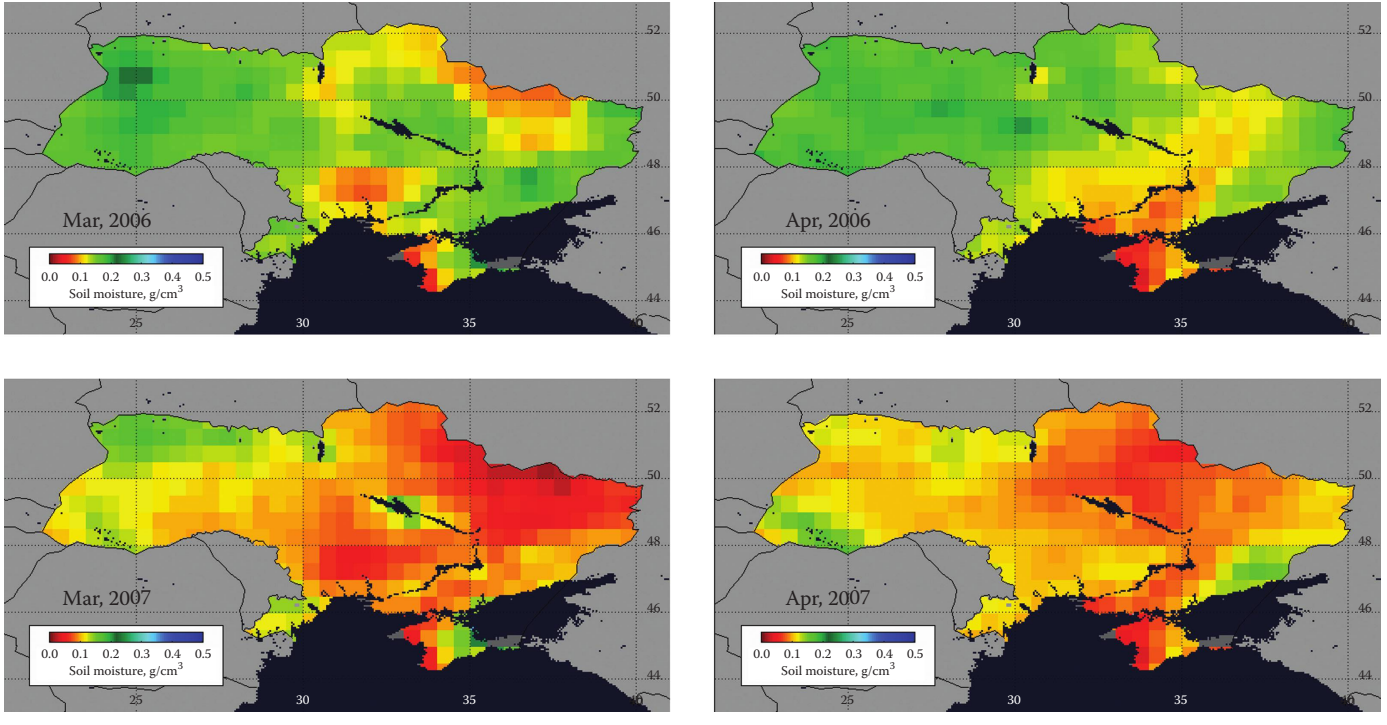

FIGURE 15.9 Monthly average soil moisture over Ukraine for the months of March and April of 2006 and 2007. Soil moisture was retrieved from AMSR-E Aqua data.